

Time to failure of hierarchical load-transfer models of fracture

M. Vázquez-Prada

Departamento de Física Teórica, Universidad de Zaragoza, 50009 Zaragoza, Spain

J. B. Gómez

Departamento de Ciencias de la Tierra, Universidad de Zaragoza, 50009 Zaragoza, Spain

Y. Moreno* and A. F. Pacheco

Departamento de Física Teórica, Universidad de Zaragoza, 50009 Zaragoza, Spain

(Received 13 April 1999)

The time to failure, T , of dynamical models of fracture for a hierarchical load-transfer geometry is studied. Using a probabilistic strategy and juxtaposing hierarchical structures of height n , we devise an exact method to compute T , for structures of height $n + 1$. Bounding T , for large n , we are able to deduce that the time to failure tends to a nonzero value when n tends to infinity. This numerical conclusion is deduced for both power law and exponential breakdown rules. [S1063-651X(99)03309-7]

PACS number(s): 64.60.Ak, 64.60.Fr, 05.45.-a, 91.60.Ba

I. INTRODUCTION

Fracture in heterogeneous materials is a complex physical problem for which a definite physical and theoretical treatment is still lacking. By “heterogeneous material” we understand a system whose breaking properties (e.g., strengths, lifetimes) depend on time and/or space in a random way [1]. This randomness arises from the many-body interactions among the constituent parts of the system, each one having mechanical properties that can be considered independent of—or at least weakly correlated with—the properties of neighboring parts. The term disordered systems is also used as a collective name for this kind of material. The presence of disorder alters radically the way the rupture process evolves compared to the single-crack growth mechanism operating in homogeneous materials (such as glass or alloys). In heterogeneous material (composites, ceramics, rocks, concrete) the process of rupture begins with delocalized damage affecting the bulk of the material, and consisting of an enormous number of microcracks nucleated at random inside the system. This population of microcracks evolves with time by coalescence and growth of individual microcracks until the final rupture point of the system is reached. In the very final stages, the process of coalescence gives rise to a single (or a few) dominant crack(s) responsible for the macroscopic failure of the material.

The analytical or even complete numerical solution of this complex problem is prohibitive. Nevertheless, our understanding of fracture in heterogeneous material has improved recently with the development of simple algorithms to simulate the breaking process. Most of these algorithms are based on percolation theory [3] and include models of random resistor networks [4], spring networks [5], and beam networks [6]. The standard way of solving these models is through a more or less dense sampling of failure space via Monte Carlo

simulation. But fracture in heterogeneous materials is, from a statistical viewpoint, a process critically dependent on the tails of the failure distribution and these tails are naturally difficult to sample using conventional Monte Carlo methods. It is thus very important to develop a set of simple models which can be analyzed either analytically or numerically, with precision and with clear asymptotic behavior, in order to guide our understanding of more complex models.

The load-transfer models belong to this group of simple, stochastic fracture models amenable to either close analytical or fast numerical solution, and whose output, spanning many orders of magnitude in sample size, allows a precise characterization of the asymptotic behavior. The collective name given to this type of model is fiber-bundle models (FBM), because they arose in close connection with the strength of bundles of textile fibers [7,8]. Since Daniels’ and Coleman’s seminal works, there has been a long tradition in the use of these simple models to analyze failure of heterogeneous materials.

FBM come in two “flavors,” static and dynamic. The static versions of FBM simulate the failure of materials by quasistatic loading, i.e., by a steady increase in the load over the system up to its macroscopic failure. One of the basic outputs is precisely the value of this ultimate strength. Time plays no role in these models, load σ is the independent variable, and the strength of each element is considered to be an independent identically distributed random variable. On the other hand, the dynamic FBM simulate failure by stress-rupture, creep-rupture, static-fatigue, or delayed-rupture, i.e., a (usually) constant load is imposed over the system and the elements break by fatigue after a period of time. The time elapsed until the system collapses is the lifetime or time to failure of the set. Time acts as the independent variable, and the lifetime of each element is an independent identically distributed random quantity.

There are three basic ingredients common to all FBM: first, a discrete set of N elements located on the sites of a d -dimensional lattice; second, a probability distribution for the failure of individual elements; and, third, a load-transfer

*On leave from Departamento de Física, Technological University of Havana, ISPJAE, Havana 19390, Cuba.

rule which determines how the load carried by a failed element is to be distributed among the surviving elements in the set.

The most common probability distribution function (second ingredient) used to express the breaking properties of individual elements is the Weibull distribution [9]. For the static cases, where the load, σ , is the independent variable, failure statistics are described by the function $P(\sigma) = 1 - \exp\{-(\sigma/\sigma_0)^\rho\}$. Here, σ_0 is a reference strength and ρ is the so-called Weibull index or shape parameter, which in essence controls the variance in the strength thresholds. For the dynamic cases, with time as the independent variable, things are more complicated because the failure of each element is sensitive to both the elapsed time *and* its load history. The probability $P(t; \sigma(t))$ of a single element failing at time t after suffering the load history $\sigma(t)$ is of the form [8]

$$P(t; \sigma(t)) = 1 - \exp\left\{-\int_0^t \kappa_j[\sigma(\tau)] d\tau\right\}, \quad (1.1)$$

where $\kappa_j(x)$, $j=1,2$, is the hazard rate or breaking rule. To impart to Eq. (1.1) the commonly observed Weibull behavior of real materials under constant load, a *power-law breaking rule* is used [10]:

$$\kappa_1(\sigma) = \nu_0 \left(\frac{\sigma}{\sigma_0}\right)^\rho. \quad (1.2)$$

Here, ν_0 is the hazard rate (number of casualties per unit of time) under the unit load σ_0 . For constant load, inserting Eq. (1.2) into Eq. (1.1) gives the Weibull probability distribution function for the dynamic FBM:

$$P(t; \sigma) = 1 - \exp\left\{-\nu_0 \left(\frac{\sigma}{\sigma_0}\right)^\rho t\right\}. \quad (1.3)$$

The widespread use of Weibull statistics stems from the experimental fact that real materials follow very closely Weibull probability distribution functions for both the strength and the time to failure of the individual elements [7,8,11,12].

Besides the power-law breaking rule, Eq. (1.2), another popular assumption in composites fracture is the *exponential breaking rule*,

$$\kappa_2(\sigma) = \phi \exp\left[\eta \left(\frac{\sigma}{\sigma_0}\right)\right], \quad (1.4)$$

where ϕ and η are two positive constants (the amplitude and the characteristic scale of the exponential function). This breaking rule has a theoretical support in the apparent necessity of a Boltzmann factor in the load (stress) for any thermally activated process (as fracture at the molecular level is interpreted [11]). The substitution of Eq. (1.4) into Eq. (1.1) does not give a Weibull function. Nevertheless, the established use of the two breaking rules makes it necessary to take both into account, and so we have dedicated Sec. V to the discussion of the lifetime of sets under the exponential breaking rule.

The most critical of the three basic ingredients of all FBM is the *load-transfer rule*, where a great deal of the physics of the models is hidden. Three end members are of interest

here: the equal load-sharing (ELS) rule, the local load-sharing (LLS) rule, and the hierarchical load-sharing (HLS) rule. In the ELS rule, which can be thought of as a mean-field approximation, the load supported by failing elements is shared equally among all surviving elements. In the LLS rule, the load of failing elements is accommodated by a neighborhood whose exact definition depends on the geometry and dimensionality of the underlying lattice. In the HLS rule the scheme of load transfers follows the branches of a fractal (Cayley) tree with a constant coordination number. Common to all three load-transfer modalities is the fact that broken elements carry no load.

ELS models have been used to predict failure under tension in elastic yarns and cables with little or no twist, because in these arrangements the load supported by a failing fiber or cable strand is shared equally by all the remaining fibers or strands in the bundle. The conjunction of a loose arrangement and a load under tension facilitates this global-range load redistribution scheme.

LLS models have their natural field of application in the failure of composite materials, and more specifically in fiber-reinforced composites with brittle fibers embedded in a stiff matrix [13]. There, as fiber breaks appear, the matrix serves the important function of transferring the shear traction generated in the matrix at the point of a fiber break to the neighboring fibers, with most of the load going to the nearest neighbors. This arrangement results in a very short-range load redistribution, both laterally across fibers and longitudinally along the fiber axis.

More important from a geophysical point of view and for this paper is the HLS rule recently introduced by Turcotte and collaborators in the seismological literature [14]. In this load-transfer modality the scale invariance of the fracture process is directly taken into account by means of a hierarchical load-transfer scheme following the branches of a fractal tree. An important property of the HLS scheme is that the zone of stress transfer is equal in size to the zone of failure, and this nicely simulates the Green's function associated with the elastic distribution of stress adjacent to a rupture [15]. The fractal tree structure used to redistribute loads is a mere construction useful to envisage the way loads from breaking elements are transferred to unbroken elements. A basic aspect of the topology of the hierarchical structure is the number of elements directly linked together; this defines the coordination, c , of the tree. That is, c fibers could be assembled to form a bundle which would behave as if it were itself a fiber. Then, c of these second-generation fibers could themselves be assembled to form a bundle which would act as a third-generation fiber, and so on. This hierarchical assemblage can be continued indefinitely and an index n is used to describe the level within the hierarchy or, equivalently, the height in the tree structure. So $n=0$ refers to the individual elements in the system, $n=1$ refers to the first level in the tree, etc. For $c=2$, $n=0$ implies individual elements, $n=1$ implies pairs of elements, $n=2$ pairs of pairs of elements, etc. Thus, an n th-order tree with coordination number c would contain $N=c^n$ elements.

Although we would stress below the importance of the analytical solution of the FBM, it is enlightening to show how these models can be solved using Monte Carlo techniques because that would facilitate the understanding of

TABLE I. Main asymptotic results for the three standard modalities of FBM in the static and dynamic cases.

	ELS	LLS	HLS
Static	Critical point	No critical point	No critical point
	$\sigma_c = e^{-1/\rho}$	$\sigma_c \propto 1/\ln N$	$\sigma_c \propto 1/\ln \ln N$
	Daniels [7]	Harlow [18]	Newman and Gabrielov [22]
Dynamic	Critical point	No critical point	Critical point
	$T_c = 1/\rho$		
	Coleman [10]	Kuo and Phoenix [20]	This paper

parts to follow. We will focus on the *dynamic* FBM, as this is the type of problem we want to address in this paper. Consider a set of N elements arranged on the sites of a lattice. The general Monte Carlo recipe goes as follows: (i) Assign random lifetimes t_i to the $i = 1, \dots, N$ individual elements, as drawn from Eq. (1.1) under unit load; (ii) advance time an amount equal to the lifetime of the shortest-lived nonfailed element in the set, say δ ; (iii) reduce lifetimes of all remaining elements by an amount $\kappa(\sigma_i)\delta$, where $\kappa(x)$ is either the power-law or the exponential breaking rule; (iv) transfer load from the failing element to other sound elements in the set according to a preset load-transfer rule (ELS, LLS, or HLS); (v) proceed to step (ii) if at least one element is unbroken, or end if the system has collapsed; (vi) add together all the individual δ 's to obtain the time to failure T of that particular realization of the system. This way of applying the Monte Carlo method is what we will refer to as the *standard method*.

Among the different results that one can obtain from the analytical or numerical solution of the fiber-bundle models (for a review, see [2]), here we are mainly interested in the asymptotic strength (static FBM) and asymptotic time to failure (dynamic FBM) of the system. The asymptotic strength is defined as the maximum load that an infinite system can support before all its elements break. The asymptotic time to failure or lifetime is the minimum time one has to wait until an infinite system collapses by all its elements breaking by fatigue. These are themselves important questions from an engineering point of view. Table I gathers the main asymptotic results for the different FBM, including the dynamic HLS model, to which this paper is dedicated. It has been known since the work of Daniels [7] that the static ELS fiber-bundle model has a critical point in the sense that for an infinite system there is a zero probability of breaking the system when applying a load σ less than a critical value σ_c , and a probability equal to 1 to break the system if the applied load is bigger than the critical load. This is valid for any probability distribution function satisfying some very mild conditions [7]. The critical strength σ_c quoted in Table I is only valid, however, for a Weibull function. As for the dynamic ELS model, Coleman [8] proved rigorously a comparable result, namely that there exists a critical time T_c below which an infinite system under dynamic rules has a zero probability of collapsing and above which the system collapses with a probability of 1. T_c varies with the assumed probability distribution function, but otherwise the critical-point result is independent of it (the value quoted in Table I is for a power-law breaking rule). Smith and Phoenix [16] give a summary of the main asymptotic results for the static

and dynamic ELS FBM. Regarding the asymptotic properties of the LLS models, the work of Smith and co-workers and of Harlow, Phoenix, and co-workers has been fundamental. They proved that neither the static nor the dynamic LLS FBM have a critical point. For the static case, the strength of the system goes to zero as the size of the system is increased. More specifically, $\sigma_c \propto 1/\ln N$ (conjectured by Harlow, Phoenix, and Smith [17]; proved by Harlow [18]). For the dynamic case a similar result holds (conjectured by Tierney [19]; proved by Kuo and Phoenix [20]). See [21] for a review of the static LLS models.

The static HLS model was shown to lack a critical point by Newman and Gabrielov [22]. In this case the reduction to zero of strength in relation to system size is very slow, $\sigma_c \propto 1/\ln \ln N$, but strictly speaking the strength of an infinite system is zero. The dynamic HLS model was introduced in the geophysical literature in Ref. [23]. Afterwards, Newman *et al.* [15] used this dynamic HLS model with the specific aim of finding out if the chain of partial failure events preceding the total failure of the set resemble a log-periodic sequence. This was motivated by the amazing fit of this type obtained in Ref. [24] to data of the cumulative Benioff strain released in magnitude > 5 earthquakes in the San Francisco Bay area before the October 17, 1989 Loma Prieta earthquake. In the analysis of [15], it appeared that, contrary to the static model, the dynamic HLS model seemed to have a nonzero time to failure as the size of the system tends to infinity. This issue was also studied in [25] by using a renormalization approach. This behavior seems odd because, as Table I shows, there is a symmetry, for a specific load transfer rule, between the static and the dynamic cases: the ELS models have a critical point both for the static and the dynamic cases; the LLS models have no critical point behavior either for the static or the dynamic case. The static HLS model has no critical point, and so it would seem natural that the dynamic HLS would not have a critical point either. Here we present an exact iterative method to compute the time to failure of sets of elements with a hierarchical modality of load transfer. (A preliminary account of the behavior of the dynamic HLS model under the power-law breaking rule has been recently published [26].) Due to the fact that the exact method is too time consuming to yield useful asymptotic results, we also present here rigorous upper and lower bounds to the lifetime of large dynamic HLS sets. From the behavior of the lower bound we conclude that the dynamic HLS model has indeed a critical point, that is, its time to failure is nonzero for an infinite system.

This paper is organized as follows. In Sec. II we review the continuous formulation of the ELS model given by Cole-

man [8]. This is useful for understanding the probabilistic approach used in the rest of the paper. This approach is compared with the standard method in a Monte Carlo simulation, to illustrate that both are equivalent. Section III contains the core of the iterative method to exactly calculate the time to failure of dynamical HLS sets. The strategy of the juxtaposition of configurations is explained and the need of defining ‘‘replica’’ configurations is introduced. This leads to the concept of *primary diagram* from which the value of the δ 's and of T , for a given n , are exactly calculated. From a primary diagram one obtains an easier one called *reduced diagram*, which is used to build the primary diagram of the next level $n+1$. In Sec. IV, aiming at simplification, we introduce the concept of *effective diagram*, as the averaged form of a primary. In these diagrams each stage of breaking is represented by a unique effective configuration whose decay width is obtained by an appropriate average of the various decay widths existing in the primary. Depending on the type of means used, upper or lower bounds for the T of the next height are obtained. So far the power-law breaking rule is used in the quantitative calculations. Section V is devoted to the exponential breakdown rule specifics. Two Appendixes have been added: In Appendix A we detail the number of replicas demanded for a general coordination, c ; in Appendix B, we show the reason why the three types of means used in the averaging effectively work to provide rigorous bounds.

II. ELS MODEL. THE PROBABILISTIC APPROACH

In Ref. [8], in the context of his statistical theory for the time dependence of mechanical breakdown in bundles of fibers at constant total load, Coleman defines an ‘‘ideal bundle’’ as one fulfilling precisely the same premises as the ELS model presented in Sec. I. Following the work of this author, let us call N the size of the bundle (or set) at $t=0$ and $n(t)$ the number of filaments (or elements) which survive to t without breaking; the lifetime, T , of the bundle is defined as the time required for $n(t)$ to reach zero. We will call σ_o the fixed load attributed to every single element at $t=0$. The hypothesis of the ELS model implies that the actual load in a particular unbroken filament at time t is

$$\sigma = \frac{\sigma_o N}{n(t)}. \quad (2.1)$$

Thus the lifetime of a very large ideal bundle formed by fibers of equal length, l , may be calculated from

$$-\frac{dn}{dt} = nl\kappa(\sigma), \quad (2.2)$$

where $\kappa(\sigma)$ is a phenomenological function. The product $l\kappa$ is called the hazard rate. In polymeric fibers, κ can be satisfactorily represented by an exponential function of σ :

$$\kappa(\sigma) = \frac{e^{\beta\sigma}}{a}, \quad (2.3)$$

where a and β are parameters that determine the behavior of the fibers under any load σ . Equation (2.3) represents the so-called *exponential breakdown rule*. An alternative also widely used is the so-called *power-law breakdown rule*:

$$k(\sigma) = \frac{1}{a} \left(\frac{\sigma}{\sigma_o} \right)^\rho. \quad (2.4)$$

From Eqs. (2.1), (2.2), and (2.3) with $x = (\beta\sigma_o N)$ and n , and the conditions $n(0) = N$ and $n(T) = 0$, one deduces

$$T = \frac{a}{l} \int_{\beta\sigma_o}^{\infty} \frac{dx e^{-x}}{x} = -\frac{a}{l} E_i(-\beta\sigma_o). \quad (2.5)$$

Using Eq. (2.4) instead of Eq. (2.3), one obtains

$$T = \frac{(a/l)}{\rho}. \quad (2.6)$$

Equation (2.2) is similar to a radioactivity equation in which $l\kappa$ stands for the decay rate, Γ , of one nucleus. In the ELS case it is not of much interest to lose this elegant continuous formulation. However, for other load-transfer schemes, such as the HLS, this analogy with radioactivity is useful, but similar continuous differential equations cannot be formulated anymore. Thus, the discrete version of this probabilistic philosophy applicable to any load-transfer scheme was developed in Ref. [27] and will be used throughout this paper. It represents an alternative to what we have called the standard method [15] commented on in Sec. I, in which the random thresholds for breaking are assigned at the beginning and the process of breaking is henceforth completely deterministic. Both points of view are equivalent. In the following we will use nondimensional magnitudes. In particular,

$$(a/l) = 1, \quad \sigma_o = 1, \quad \text{and} \quad \beta\sigma_o = 1. \quad (2.7)$$

Note that this would be equivalent to adopting, with the notation of Sec. I, $\nu_o = \sigma_o = \phi = \eta = 1$.

In the probabilistic approach [27], in each time increment, defined as

$$\delta = \frac{1}{\sum_j \Gamma_j}, \quad (2.8)$$

one element of the sample decays. The index j runs along all the surviving elements. Using Eqs. (2.3), (2.4), and (2.7), we have

$$\Gamma_j = \sigma_j^\rho \quad (\text{or} \quad \Gamma_j = e^{\sigma_j}). \quad (2.9)$$

The probability of the specific element, m , to fail is

$$p_m = \Gamma_m \delta. \quad (2.10)$$

Equation (2.8) is the ordinary link between the mean time interval for one element to decay in a radioactive sample and the total decay width of the sample. The time to failure, T , of a bundle (set of elements) is the sum of the N δ 's.

It is instructive to apply Eq. (2.8) to the ELS case where Γ_j does not depend on j because every surviving element bears the same load. Here, in the k th time step, the number of survivors is $n_k = N - k$ and the individual load is $\sigma_k = N/(N - k)$. Then for the power-law rule,

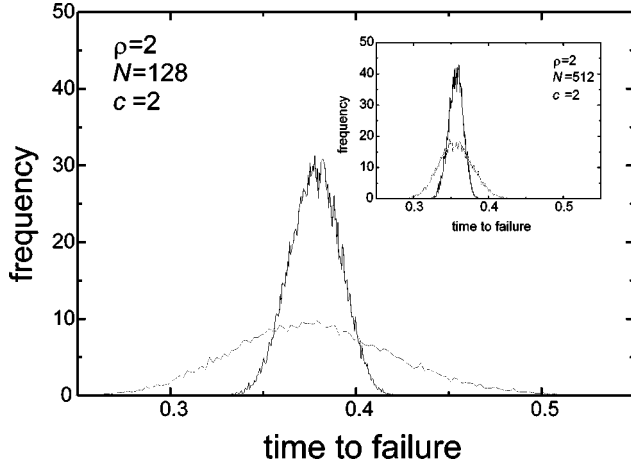


FIG. 1. Comparison of Monte Carlo simulations; the broad distributions come from using the standard approach, and the thinner distributions come from using the probabilistic approach. The time to failure is plotted in dimensionless units.

$$\delta_k = \frac{1}{N-k} \frac{(N-k)^\rho}{N^\rho} = \frac{(N-k)^{\rho-1}}{N^\rho},$$

with $k=0, \dots, N-1$ and

$$T = \sum_{k=0}^{N-1} \delta_k. \quad (2.11)$$

If $\rho=2$, $T = \frac{1}{2}(1 + 1/N)$. For a general value of ρ , using Stolz's theorem [28] we find

$$\lim_{N \rightarrow \infty} T = \frac{(N-1)^{\rho-1}}{N^\rho - (N-1)^\rho} \rightarrow \frac{1}{\rho}, \quad (2.12)$$

which coincides with Eq. (2.6).

When dealing with the exponential breakdown rule, proceeding analogously one easily checks that the sum of the series of δ 's, for sufficiently high N , provides the same result as the exponential integral of Eq. (2.5).

It is also instructive to compare the results obtained from Monte Carlo simulations in the calculus of T in two ways: (a) by using the standard procedure, i.e., of assigning random individual lifetimes at the beginning of each simulation and proceeding deterministically; or (b) by using a probabilistic point of view, i.e., from Eq. (2.8) and Eq. (2.10). This comparison is shown in Fig. 1 for HLS sets of $N=128$ and $N=512$ elements (with $c=2$, $\rho=2$). Note the significant reduction in the dispersion thickness obtained by using this second method. This contrast tends to decrease for growing N and growing ρ . Obviously, the Monte Carlo strategy can be applied for any modality of load transfer in the framework of the probabilistic method. The inconvenience lies in the very essence of these simulations, i.e., their moderate accuracy and large cost for large sets. In this paper, we will show how to apply the probabilistic method to the HLS transfer modality, in order to obtain an exact algebraic method for the lifetimes, and how to explore the asymptotic values of T when N tends to infinity.

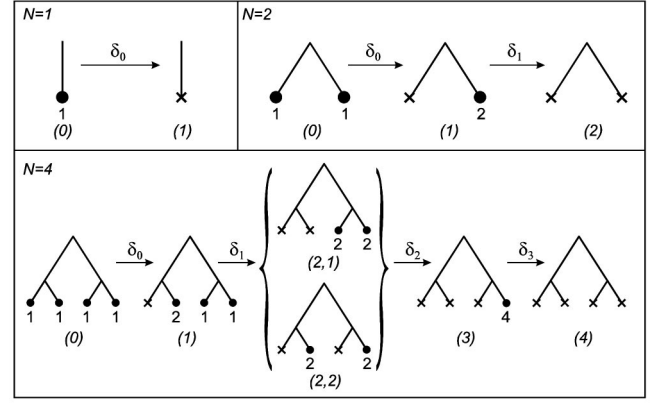


FIG. 2. Breaking process for the three smallest trees of coordination $c=2$ ($N=1,2,4$). The integers in parentheses (r) represent the number of breakings that occurred. The δ s stand for the time elapsed between successive individual breakings and the numbers under the legs indicate the load they bear.

III. EXACT ITERATIVE METHOD FOR HLS DYNAMICAL MODELS

To give a perspective of what is going on in the rupture process of a hierarchical set, we have drawn in Fig. 2 the three smallest cases for trees of coordination $c=2$. Denoting by n the number of levels, or height of the tree, i.e., $N=2^n$, we have considered $n=0, 1$, and 2 . The integers within parentheses (r) account for the number of failures existing in the tree. When there are several nonequivalent configurations corresponding to a given r , they are labeled as (r,s) , i.e., we add a new index s . The total load is conserved except at the end, when the tree collapses. Referring to the high symmetry of loaded fractal trees, note that each of the configurations explicitly drawn in Fig. 2 represents all those that can be brought to coincidence by the permutation of two legs joined at an apex, at any level in the height hierarchy. Hence we call them nonequivalent configurations or merely configurations. In general, each configuration (r,s) is characterized by its probability $p(r,s)$, $\sum_s p(r,s)=1$, and its decay width $\Gamma(r,s)$. The time step for one-element breaking at the stage r is given by

$$\delta_r = \sum_s p(r,s) \frac{1}{\Gamma(r,s)}. \quad (3.1)$$

This is the necessary generalization of Eq. (2.8) due to the appearance, for the same r , of nonequivalent configurations during the decay process of the tree. In cases of branching, the probability that a configuration chooses a specific direction is equal to the ratio between the partial decay width in that direction and the total width of the parent configuration. And the probability of a given configuration $p(r,s)$ is given by the sum, extended to all its possible parents, of the product of the probability of each parent times the probability of choosing that specific direction.

We will compute at a glance the δ 's of Fig. 2 in order to analyze the general case later. To be specific, we will always use $\rho=2$. For $n=0$, we have $\Gamma(0)=1^2$ and $\delta_0=1/1^2=1=T$. For $n=1$, $\Gamma(0)=1^2+1^2=2$, $\delta_0=\frac{1}{2}$; $\Gamma(1)=2^2$, $\delta_1=\frac{1}{4}$; and hence $T=\frac{1}{2}+\frac{1}{4}=\frac{3}{4}$. For $n=2$, $\Gamma(0)=1^2+1^2+1^2$

$+1^2=4$, $\delta_0=\frac{1}{4}$; $\Gamma(1)=2^2+1^2+1^2=6$, $\delta_1=\frac{1}{6}$. Now we face a branching; the probability of the transition $(1) \rightarrow (2,1)$ is $\frac{4}{6}$ and the probability of the transition $(1) \rightarrow (2,2)$ is $\frac{2}{6}$; on the other hand, $\Gamma(2,1)=2^2+2^2=8=\Gamma(2,2)$, hence $\delta_2=\frac{4}{6} \times \frac{1}{8} + \frac{2}{6} \times \frac{1}{8} = \frac{1}{8}$. Finally $\delta_3=\frac{1}{16}$ and the addition of δ 's gives $T=\frac{29}{48}$.

Now we define the *replica* of a configuration belonging to a given n , as the same configuration but with the loads doubled (this is because we are using $c=2$). The replica of a given configuration will be recognized by a prime sign. In other words, $(r,s)'$ is the replica of (r,s) . Note that when a configuration represents the state of complete collapse, it and its replica are the same thing. When dealing with the power-law breakdown rule, any decay width, partial or total, related to $(r,s)'$ is automatically obtained by multiplying the corresponding value of (r,s) by the common factor $c^\rho=2^\rho=4$. This also implies that $p(r,s)=p(r,s)'$. In the exponential rule, this does not work and the widths of the replicas have to be specifically calculated (this is explained in Sec. V). The need to define the replicas stems from the observation that any configuration appearing in a stage of breaking r of a given n is built as the juxtaposition of two configurations of the level $n-1$, including also the replicas of the level $n-1$ as ingredients of the game. In Fig. 2, one can observe the explicit structure of the configurations of $N=4$ (or of $N=2$) as a juxtaposition of those of $N=2$ (or of $N=1$) and its replicas. From this perspective, we notice that the total number of configurations appearing in the fracture process of a tree of height n (omitting the totally collapsed one), \mathcal{N}_n , is equal to

$$\mathcal{N}_n = \frac{\mathcal{N}_{n-1}(\mathcal{N}_{n-1} + 1)}{2} + \mathcal{N}_{n-1}.$$

In this formula the first term represents all the possible combinations (with repetition) of pairs of ordinary configurations of the height $n-1$. The second term represents the configurations formed by juxtaposing a collapsed tree of height $n-1$ together with any of the \mathcal{N}_{n-1} replicas of the previous height. Thus,

$$\mathcal{N}_n = \frac{\mathcal{N}_{n-1}(\mathcal{N}_{n-1} + 3)}{2}. \tag{3.2}$$

Feeding $\mathcal{N}_0=1$ into Eq. (3.2), we obtain $\mathcal{N}_1=2$, $\mathcal{N}_2=5$, $\mathcal{N}_3=20$, $\mathcal{N}_4=230$, $\mathcal{N}_5=26\,795$, $\mathcal{N}_6 \approx 3.59 \times 10^8$, $\mathcal{N}_7 \approx 6.45 \times 10^{16}$, etc. It is clear that the amount of configurations to deal with soon constitutes an insurmountable problem.

The single-element breaking transitions in configurations of height n can be only of three types. Type *a* transitions correspond to the breaking of one element in half of the tree while the other half remains as an unaffected spectator. Type *b* transitions correspond to the decay of the last surviving element in one-half of the tree, which provokes its collapse and the corresponding doubling of the load borne by the other half. In these two cases, the transition width coincides with that already obtained when solving the level $n-1$. Finally, type *c* transitions correspond to the scenario in which one-half of the tree has already collapsed and in the other half one breaking occurs. In this third case, the decay width is that of a replica of the level $n-1$, which, as said before, is

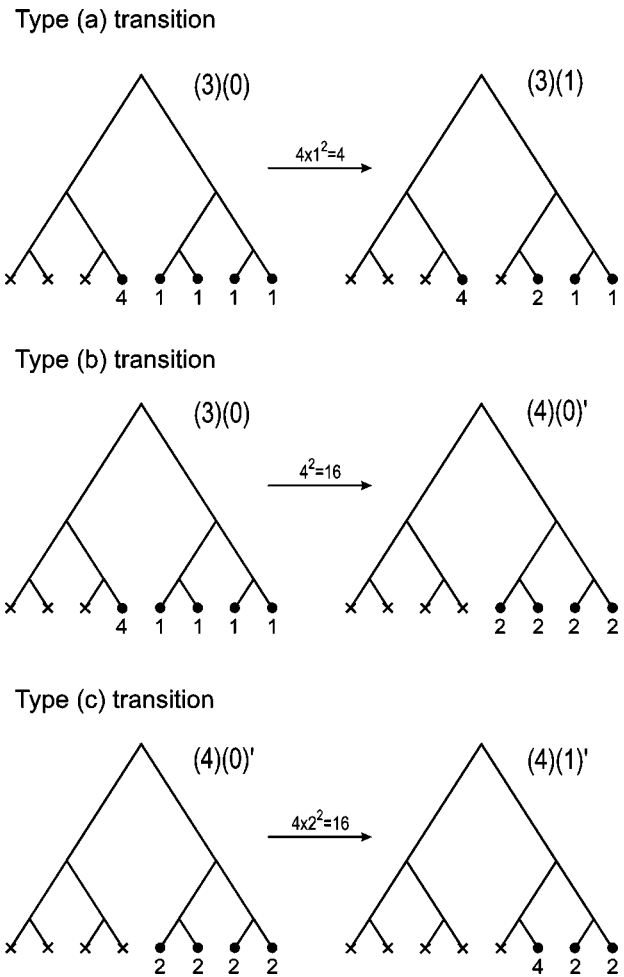


FIG. 3. Calculation of three partial decay widths in $n=3$, from the information obtained in $n=2$.

a common factor c^ρ times the ordinary width. This holds for any height n and allows the computation of all the partial decay widths in a tree of height n from those obtained in the height $n-1$. This is illustrated in Fig. 3 for the three types of transitions for trees with $n=3$ ($\rho=2$ has been used).

In Fig. 2 and Fig. 3 we have drawn the different configurations of low n explicitly, that is, by representing them as small fractal trees at different stages of damage. It is convenient, for reasons of economy, to introduce a symbolic notation for the configurations so that the complete process of breaking of a tree of height n adopts a more compact look. This is shown in Fig. 4. There, the different configurations of $n=3$ are labeled by the integers within the boxes. The two parentheses at their right, with their respective integers, represent the two $n=2$ juxtaposed configurations forming that of level $n=3$. This information of the previous height will be called the *genealogy*. Time is assumed to flow downwards. The numbers accompanying an arrow connecting two boxes stand for the decay width of that transition. Coming back to Fig. 3 one recognizes there that those explicit transitions are nothing else but what in Fig. 4 is represented as block 3,1 \longrightarrow block 4,2, block 3,1 \longrightarrow block 4,1, and block 4,1 \longrightarrow block 5,1. A diagram like that of Fig. 4 is called a *primary*, because it is formed by the juxtaposition of all possible configurations of the previous height. Thus,

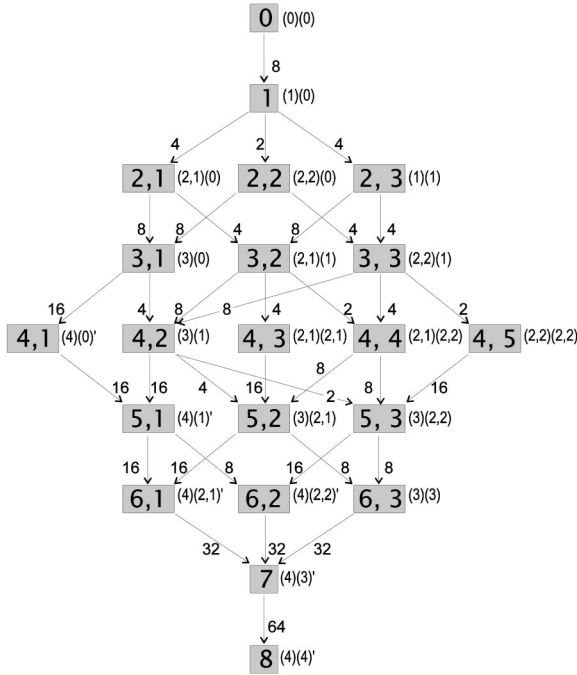


FIG. 4. Symbolic representation of the gradual rupture of the tree of height $n=3$ ($c=2, \rho=2$). Time flows downwards.

each configuration belonging to a primary diagram has a specified genealogy. This allows the computation of all the decay widths of the diagram. As foreseen in Eq. (3.2), not counting the totally collapsed configuration, $\mathcal{N}_3=20$. The sum of all the partial widths of a parent configuration in a branching is always equal to the total decay width, Γ , of the parent. From this primary width diagram one deduces the probability of any primary configuration at any stage r of breaking, and consequently δ_r is obtained using Eq. (3.1). Finally, by adding all the δ 's we calculate $T(n=3)$.

After a primary diagram has been obtained, i.e., after calculating all its decay widths, it can be simplified. The idea is to fuse, at each r , all the configurations having the same total decay rate, Γ . Once fused, these configurations have a probability equal to the sum of the old probabilities, and obviously maintain the same Γ . A primary diagram simplified in this way will be called a *reduced* diagram. An element of a reduced diagram resulting from a fusion has no genealogy in the sense that it does not derive from one but from several juxtapositions. The genealogy was used in the calculation of the primary diagram. The later fusion does not require any other independent information. To illustrate the concept of what a reduced diagram is, let us look again at Fig. 2. For $n=0$ and $n=1$, for each r there is only one configuration and hence primary and reduced diagrams are identical. For $n=2$, for $r=2$ there are two configurations in the primary diagram, but they have the same width, specifically, for $\rho=2$, $\Gamma(2,1)=\Gamma(2,2)=8$. Thus these two configurations can be fused and the resulting effective diagram is a chain of five elements, i.e., the branching disappears. Performing this task with the $n=3$ of Fig. 4, one would obtain the reduced diagram of Fig. 5. The total number of configurations appearing in the reduced diagrams, \mathcal{N}'_n , does not derive from a closed formula as occurs with \mathcal{N}_n . However, it can easily be de-

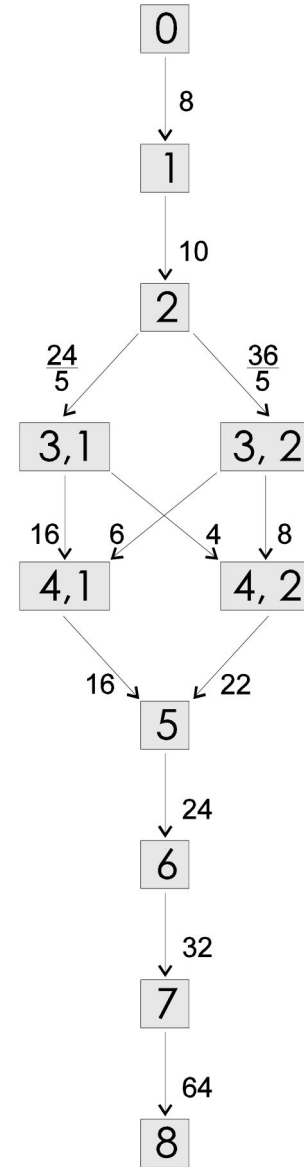


FIG. 5. Result of ‘‘reducing’’ the diagram of Fig. 4.

rived by means of the computer to obtain $\mathcal{N}'_1=1$, $\mathcal{N}'_2=2$, $\mathcal{N}'_3=10$, $\mathcal{N}'_4=36$, $\mathcal{N}'_5=202$, $\mathcal{N}'_6=1669$, $\mathcal{N}'_7=16408$. The important point is that one can use a reduced diagram of the level n to build a primary of the level $n+1$ obtaining the exact information of the new level. After calculating that primary, by fusing again configurations of equal Γ , one would obtain the reduced diagram of the height $n+1$.

By iterating this procedure, that is, by forming the primary diagram of the $n+1$ height by juxtaposing the configurations of the reduced diagram of the height n , we can, in principle, exactly obtain the total time to failure of trees of successively doubled size. In spite of the great simplification obtained when using reduced diagrams, the problem of dealing with a vast amount of configurations still remains. This fact eventually blocks the possibility of obtaining exact results for trees high enough as to be able to gauge the asymptotic behavior of T in HLS sets. A few examples of exact results, for $c=2$ and $\rho=2$, are $T(n=3)=\frac{63451}{123200}$, $T(n=4)=\frac{21216889046182831}{46300977698976000}$, $T(n=5)=0.420823219104814$.

The iterative procedure was programed in MATHEMATICA 3.0 with infinite precision and took 10 min CPU time for $n=5$.

IV. BOUNDS FOR THE TIME TO FAILURE OF THE HLS MODELS

As seen above, whenever in a primary diagram one fuses configurations of the same Γ , no information is lost and the calculation of the time to failure remains exact. In spite of this simplification, the magnitude of the Bayesian problem becomes huge even when dealing with a moderate n . That is why we have looked for alternative approximation procedures to estimate T . In fact, the most important goal, as explained in Sec. I, is to find out if the T of very large HLS sets tends to zero or, on the contrary, remains finite. With these points in mind, we have found that a drastic but appropriate simplification of the primary diagrams, in which one averages all the configurations of a given r into a unique configuration with an effective decay width, leads to obtaining, in the subsequent heights, values of T systematically lower (or higher) than the exact result. As this fusion leads to only one effective configuration, it will have probability 1. The value of its decay width will be called a_r . Such ‘‘chain’’ diagrams will be called *effective diagrams*. For $n=3$, this is drawn in Fig. 6. These effective diagrams, which substitute the previously defined reduced diagrams, are used exactly in the same way, i.e., to calculate a new (approximate) primary diagram of the next height. The economy obtained by using effective diagrams is obvious. As the number of effective configurations of a level $n-1$ is 2^{n-1} , the primary of height n , built from this effective diagram of height $n-1$, will have a number of configurations \mathcal{N}'' , given by

$$\mathcal{N}'' = \frac{2^{2n-2} + 3 \times 2^{n-1}}{2}; \tag{4.1}$$

that is, $\mathcal{N}''_1=2$, $\mathcal{N}''_2=5$, $\mathcal{N}''_3=14$, $\mathcal{N}''_4=44$, $\mathcal{N}''_5=152$, $\mathcal{N}''_6=560$, $\mathcal{N}''_7=2144$, etc.

It is clear that for $n=0, 1$, and 2 , the reduced diagrams and the effective diagrams are identical, i.e., $a_r = \Gamma(r)$. The point is to define a_r for $n \geq 3$ so that the $T(n \geq 4)$ are lower (or higher) than its exact result.

A trivial option is to define

$$a_r = \Gamma_{\max}(r) \quad \text{or} \quad \Gamma_{\min}(r) \tag{4.2}$$

i.e., by assuming that the only configurations formed during the breaking of the tree are those of the maximum (minimum) value of Γ . As it is easy to foresee, the use of Eq. (4.2) leads to poor bounds. In fact, the lower bound goes quickly to zero. We have found that good lower bounds are obtained by using effective diagrams where a_r is the arithmetic mean (AM),

$$a_r(\text{AM}) = \sum_s p(r,s) \Gamma(r,s), \tag{4.3}$$

or even better by using the geometric mean (GM),

$$a_r(\text{GM}) = \prod_s \Gamma(r,s)^{p(r,s)}. \tag{4.4}$$



FIG. 6. ‘‘Effective’’ diagram for $n=3$.

Good higher bounds are obtained from the harmonic mean (HM),

$$a_r(\text{HM}) = \frac{1}{\sum_s p(r,s) \frac{1}{\Gamma(r,s)}}. \tag{4.5}$$

In Appendix B, we analyze why bounds result. Note that given the primary diagram of a height n , which leads to c^n δ 's, the elements forming the effective diagram defined with the aim of obtaining higher bounds are exactly a_r

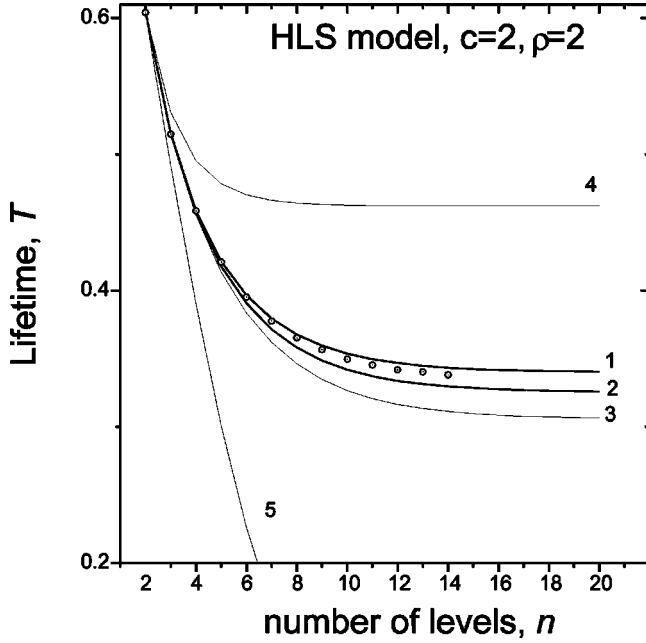


FIG. 7. Dimensionless lifetime, T , for a fractal tree of height n . The small circles are obtained from Monte Carlo simulations. Lines 4 and 1 are higher bounds based on Γ_{\min} and the HM, respectively. Lines 2, 3, and 5 are lower bounds based on the GM, AM, and Γ_{\max} , respectively.

$=1/\delta_r$. The fact that the $a_r(i)$, $i = \text{AM, GM, and HM}$, lead to bounds in the form explained above is in qualitative concordance with the inequality

$$\Gamma_{\min}(r) \leq a_r(\text{HM}) \leq a_r(\text{GM}) \leq a_r(\text{AM}) \leq \Gamma_{\max}(r), \quad (4.6)$$

which is always a mathematical fact. The bounds obtained from these formulas for $c=2, \rho=2$ are plotted in Fig. 7, together with points representing Monte Carlo results. As the bounds based on the GM and on the HM are the most stringent, they will be called T_l and T_h , respectively. The detailed behavior of T_l has been analyzed in a log-normal plot of $T_l - T_{l,\infty}$ against the number n of levels of the tree. $T_{l,\infty}$ is a constant obtained from a fit of the data points to the exponential function $ae^{-b(n-n_0)}$ shifted downwards by this amount $T_{l,\infty}$ (a , b , and n_0 are three fitting parameters of no interest here). We have performed a careful sensitivity analysis of the four-parameter exponential fitting because the success of this exponential decay to a nonzero limit is the hallmark of the claim. Table II records $T_{l,\infty}$ obtained from an exponential fit to the last k data points. The first $T_{l,\infty}$ column is for a fit using up to a maximum level of $n=20$ (hence the notation n_{\max} in the table); the second $T_{l,\infty}$ column is for the same fit but dropping the $n=20$ value; for the third $T_{l,\infty}$ column we have also dropped the $n=19$ data point. It is clear from the trend in the three $T_{l,\infty}$ columns that a saturation towards $T_{l,\infty} = 0.32537 \pm 0.00001$ occurs when using only information of big trees to perform the nonlinear fitting. A similar analysis of T_h leads to $T_{h,\infty} = 0.33984 \pm 0.00001$. The quality of this exponential fit is also shown in Fig. 8. Similar fittings of the Monte Carlo data points are inconclusive, due to the intrinsic noisiness of the MC results and the limited size of the simulated sets ($N < 2^{16}$ elements). What

TABLE II. Sensitivity analysis of the exponential decay fitting to the lower bound results.

$n_{\max}=20$		$n_{\max}=19$		$n_{\max}=18$	
k	$T_{l,\infty}$	k	$T_{l,\infty}$	k	$T_{l,\infty}$
19	0.32575	18	0.32579	17	0.32585
18	0.32551	17	0.32553	16	0.32555
17	0.32541	16	0.32542	15	0.32542
16	0.32537	15	0.32537	14	0.32538
15	0.32536	14	0.32536	13	0.32536
14	0.32536	13	0.32536	12	0.32536
13	0.32536	12	0.32536	11	0.32536
12	0.32537	11	0.32537	10	0.32536
11	0.32537	10	0.32537	9	0.32537
10	0.32537	9	0.32537	8	0.32537
9	0.32537	8	0.32537	7	0.32537
8	0.32537	7	0.32537	6	0.32537
7	0.32537	6	0.32537	5	0.32537
6	0.32537	5	0.32537		
5	0.32537				

this result implies is that a system with a hierarchical scheme of load transfer and a power-law breaking rule ($c=2, \rho=2$) has a time to failure for sets of infinite size, T_{∞} , such that $0.32537 \leq T_{\infty} \leq 0.33984$. Thus, there is an associated zero probability of failing for $T < T_{\infty}$ and a probability equal to 1 of failing for $T > T_{\infty}$. The critical point behavior is thus numerically confirmed.

V. EXPONENTIAL BREAKING RULE

When dealing with the exponential breaking rule in the probabilistic approach, one has to use Eq. (2.3) for the hazard rate function. For the specific value of the parameters as fixed in Eq. (2.7), we have

$$\Gamma_j = e^{\sigma j}. \quad (5.1)$$

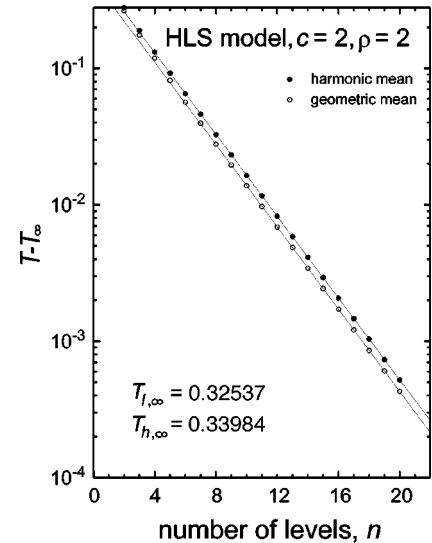


FIG. 8. Visualization of the exponential fittings to the results obtained by using geometric and harmonic means.

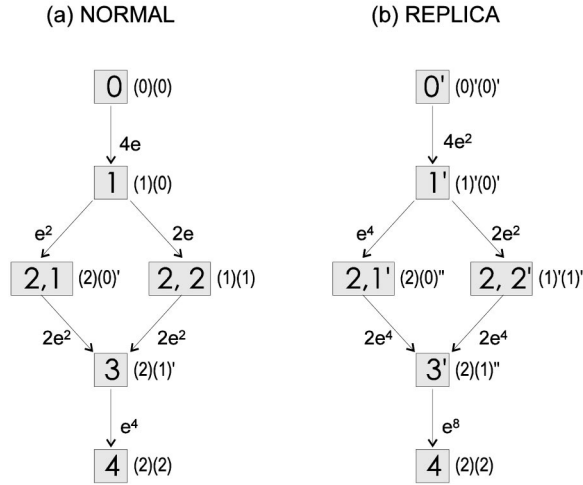


FIG. 9. Primary diagrams for the exponential breaking rule ($n=2$).

The problem with this breaking rule is that the values of the decay widths appearing in a diagram where the loads are doubled, i.e., in a diagram replica, are not obtained by multiplying the normal ones by a fixed constant, as occurred with the power-law breaking rule. This is easily checked in Fig. 9, where the primary diagram for $n=2$ and its replica are shown. The notation is equal to that of Sec. II. The values of the decay widths here are dictated by Eq. (5.1). Several comments are in order. We see that the structure of the diagrams is equal to those appearing for the power-law case because this is independent of the breaking rule assumed. In Fig. 9(b) we have drawn explicitly a replica, that is, a diagram in which the system instead of starting with individual loads, $\sigma_o=1$, starts with doubled individual loads, $\sigma'_o=2\sigma_o=2$. We also see that, just in the same way as the quantitative calculation of the primary of Fig. 9(a) required the knowledge of the information of the previous height and of its replicas, the calculation of the diagram of Fig. 9(b) requires the knowledge of the primed elements and the double-primed elements (i.e., with loads multiplied by 4) of the previous height. Thus, suppose that we want to calculate T up to the height $n=4$. This demands the knowledge of the reduced diagram of $n=3$ and of its replica. We will denote them by $\{3\}$ and $\{3\}'$. To obtain $\{3\}$ we need to know $\{2\}$ and $\{2\}'$, and to obtain $\{3\}'$ we need to know $\{2\}'$ and $\{2\}''$. Going backwards up to $n=0$, we observe that the scheme of information needed looks like the following triangular array:

$$\begin{array}{cccccc}
 \{0\} = e & \{0\}' = e^2 & \{0\}'' = e^4 & \{0\}''' = e^8 & \{0\}'''' = e^{16} & \\
 \{1\} & \{1\}' & \{1\}'' & \{1\}''' & & \\
 \{2\} & \{2\}' & \{2\}'' & & & \\
 \{3\} & \{3\}' & & & & \\
 \{4\} & & & & &
 \end{array}$$

In other words, to obtain the T of a given height n , we have to explicitly calculate the primary diagrams of the previous values of n , starting from $n=0$, up to a loading n times the usual diagram with $\sigma_o=1$. The primary diagrams of low n are calculated at once, hence the extra work with respect to the power-law case is not too much. When explaining the

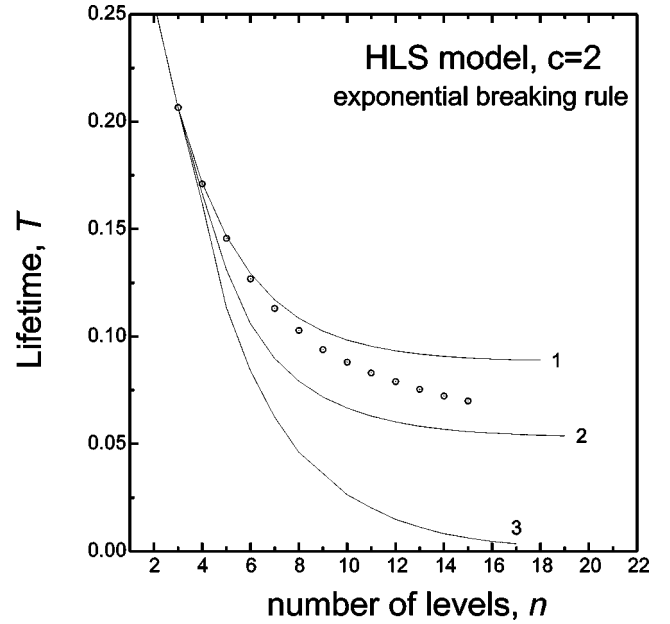


FIG. 10. Results for T from trees of height n , with the exponential breaking rule. The small circles correspond to Monte Carlo simulations. Lines 2 and 3 correspond to lower bounds based on GM and AM, respectively.

above-mentioned triangular array, we were referring to exact primary diagrams, taking for granted that our aim was to obtain exact results. Obviously this changes if our aim is the calculation of bounds; then one would proceed by averaging widths for each r , that is, by calculating means and dealing with effective diagrams.

In Fig. 10, we have drawn the lifetimes, T , for trees of height n . The circles are results obtained from Monte Carlo simulations. For the exponential breaking rule, the lower bound based on the arithmetic mean, curve (3) goes to zero. Thus the only lower bound that remains useful is that based on the geometric mean. Again, it will be called T_l . By fitting the data T_l by an exponential function of the form $T_l = T_{l,\infty} + ae^{-b(n-n_o)}$, we observe a clean saturation of the asymptotic time to failure towards $T_{l,\infty} = 0.05285 \pm 0.00001$; analogously, we obtain $T_{h,\infty} = 0.08825 \pm 0.00001$. Hence, the critical point behavior is also numerically confirmed for the exponential breaking rule.

VI. CONCLUSIONS

In this paper the time to failure, T , of hierarchical load-transfer models of fracture has been studied. Initially we have explained in detail the so-called probabilistic approach to load-transfer dynamical models as opposed to the standard approach, in which random lifetimes are assigned to the elements of the set and the process of fracture evolves deterministically. We have emphasized that when viewed from the probabilistic point of view, the calculation of T is analogous to the computation of the total decay time of a radioactive sample. In fact, the terminology of radioactivity appears throughout this paper. We have shown that the calculation of T , using Monte Carlo simulations, has a smaller dispersion if one adopts the probabilistic approach.

Then, we have devised an exact method to compute T of

hierarchical structures of size $N=c^n$. The number of elements of the set is N , c is the coordination of the tree, and n the height of the fractal tree. The method is iterative, i.e., for a given c it allows the computation of a tree of height $n+1$ once one has calculated a tree of height n . In this context, the sentence “a tree is calculated” means that one knows the value of all the partial decay widths between all possible configurations appearing during the breaking process of that tree. Once this information is known, one easily calculates the probability of reaching each configuration, and the individual values of each δ , i.e., the one-element breaking time. The key of the method derives from the observation that the structure of the configurations of the $n+1$ type is a mere juxtaposition of c configurations of the n type. In this juxtaposition, the so-called replicas also play a role. The quantitative information of how replica configurations behave is explained for the two relevant breaking rules: the power law and the exponential. In the power-law breaking rule, any decay width of a replica is just a common factor times the original value. In the exponential breaking rule, on the contrary, the decay widths of replicas have to be individually calculated.

The iterative process, including the information of the replicas, can be easily processed by a computer. It allows the exact calculation of T for moderate heights n . An exact simplification, denoted as reduction, is introduced to diminish the magnitude of the information to deal with. But even with the reduction trick, it is difficult to surpass, say $n=7$ for $c=2$. Higher values of the coordination imply smaller values for the accessible height.

Thus we conclude that exploring the behavior of T , for large n , dealing with exact results, is impossible. For this reason we have turned our interest towards developing simple approximate methods which can, however, provide interesting information on the asymptotic value of T . In this context appears the idea of obtaining bounds for T . It is found that by performing adequate averages of the decay widths appearing at each stage of breaking of a height n , the value of T obtained in the next height $n+1$ is systematically lower (or higher) than what the exact result would be. In one Appendix we have given details of why bounds result. As the results obtained from the bounds reach values beyond $n=17$ ($c=2$), one is able to explore their asymptotic behavior by a careful exponential fitting, which provides clear numerical evidence (although nonrigorous) that for $c=2$, T tends to a nonzero value when n tends to infinity. This conclusion is obtained for both the power-law and the exponential breaking rules. For the power-law hazard rate, a proof was given in [29]. Invoking conventional universality-class arguments, one deduces that this nonzero limit holds for hierarchical structures of any coordination.

ACKNOWLEDGMENTS

A.F.P is grateful to J. Asín, J. Bastero, J.M. Carnicer, and L. Moral for clarifying discussions. M.V-P. thanks Miren Alvarez for discussions. Y.M thanks the AECI for financial support. This work was supported in part by the Spanish DGICYT.

APPENDIX A: ON THE REPLICAS

We have seen in Sec. III that the knowledge of the reduced configuration of a level $n-1$ is not enough to obtain the primary diagram of the level n ; we also have to know the replica of the $n-1$ level. Expressed in the singular, this sentence is misleading. In fact, it only holds for $c=2$. One can easily check that for a general c , the number of replicas required, m , is

$$1 \leq m \leq (c-1). \quad (\text{A1})$$

In the case of the power-law breaking rule, any decay width of these replicas would be obtained by multiplying its normal value by the factor

$$\left(\frac{c}{c-m}\right)^p, \quad (\text{A2})$$

while as seen in Sec. V, the exponential breaking rule demands the individualized calculations of each replica, with its corresponding extra loading. As an example, beyond the usual $c=2$, let us consider for the case $c=4$ the process of breaking up to the collapse of the two minimum trees $n=0$ and $n=1$. Using a self-explanatory notation, we have

$$\begin{array}{l}
 n=0 \quad \boxed{1} \longrightarrow \boxed{0} \\
 \\
 n=1 \quad \begin{array}{ccccccc}
 \boxed{1} \boxed{1} & \longrightarrow & \boxed{0} \boxed{\frac{3}{4}} & \longrightarrow & \boxed{0} \boxed{0} & \longrightarrow & \boxed{0} \boxed{0} \\
 \boxed{1} \boxed{1} & & \boxed{\frac{3}{4}} \boxed{\frac{3}{4}} & & \boxed{2} \boxed{2} & & \boxed{0} \boxed{4} & \longrightarrow & \boxed{0} \boxed{0}
 \end{array}
 \end{array}$$

We see that the solution of the height $n=1$, demands the information of the decay width of block 1 but also that of block $\frac{3}{4}$, of block 2, and of block 4; i.e., for $c=4$ the iterative method requires the knowledge of three replicas, as foreseen in Eq. (A1).

APPENDIX B: ON WHY BOUNDS RESULT

Following the arguments of Secs. III and IV, one easily sees that the first δ in which there must be a discrepancy between the exact result and the approximate results coming from the use of effective diagrams is the δ_3 of $n=4$. For $c=2$, $\rho=2$, we obtain

$$\delta_3(\text{HM}) = \frac{128}{2893} = 0.044\,244\,7,$$

$$\delta_3(\text{exact}) = \frac{17}{385} = 0.044\,155\,8,$$

$$\delta_3(\text{GM}) = \frac{1}{3} \left[\frac{1}{11} + \frac{1}{8 + 20^{2/5} \times 14^{3/5}} \right] = 0.044\,107\,4, \quad (\text{B1})$$

$$\delta_3(\text{AM}) = \frac{59}{1342} = 0.0439\,642.$$

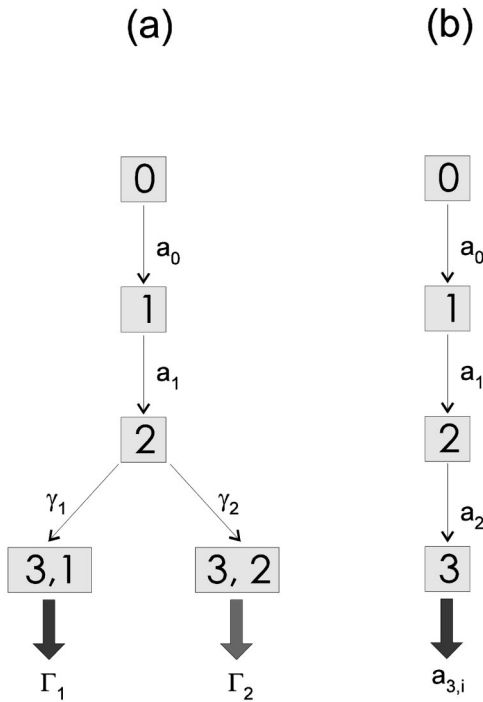


FIG. 11. Top of a failure diagram down to the fourth decay stage. (a) represents the reduced diagram and (b) the corresponding effective diagram.

This results from the fusion of the two configurations block 3,1 and block 3,2 of Fig. 5, which have a different Γ . To clarify why bounds result, let us analyze this point from a general perspective. In Fig. 11 is drawn the top of a reduced diagram of height, say, n , and at its right the corresponding effective diagram. We assume $\Gamma_1 \neq \Gamma_2$, $a_2 = \gamma_1 + \gamma_2$, and $i = \text{AM, GM, or HM}$,

$$a_{3, \text{AM}} = \frac{\gamma_1}{a_2} \Gamma_1 + \frac{\gamma_2}{a_2} \Gamma_2,$$

$$a_{3, \text{GM}} = \Gamma_1^{\gamma_1/a_2} \Gamma_2^{\gamma_2/a_2}, \quad (\text{B2})$$

$$a_{3, \text{AM}} = \frac{1}{\left(\frac{\gamma_1}{a_2}\right) \frac{1}{\Gamma_1} + \left(\frac{\gamma_2}{a_2}\right) \frac{1}{\Gamma_2}}.$$

From the reduced diagram we obtain the top of the corresponding primary of the height $n + 1$. This is shown in Fig. 12, and from the effective diagram one obtains the top of the primary shown in Fig. 13. Now let us compute the exact δ_3 coming from Fig. 12 to be compared with that (approximate) coming from Fig. 13. In Fig. 12, we have

$$p(3.1) = \frac{a_1}{a_0 + a_1} \frac{\gamma_1}{a_0 + a_2},$$

$$p(3.2) = \frac{a_1}{a_0 + a_1} \frac{\gamma_2}{a_2 + a_2},$$

$$p(3.3) = \frac{a_0}{a_0 + a_1} + \frac{a_1}{a_0 + a_1} \frac{a_0}{a_2 + a_2}.$$

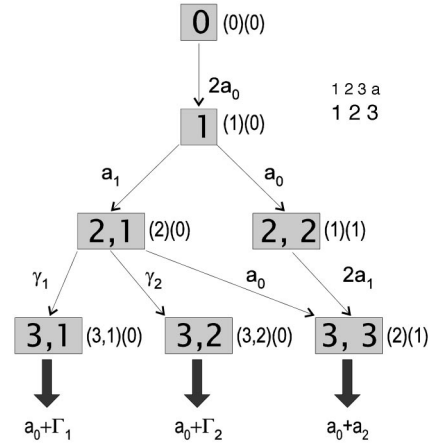


FIG. 12. Top of the primary diagram built from the reduced diagram drawn in Fig. 11 (a).

Thus

$$\delta_3(\text{exact}) = p(3.1) \frac{1}{a_0 + \Gamma_1} + p(3.2) \frac{1}{a_0 + \Gamma_2} + p(3.3) \frac{1}{a_1 + a_2}. \quad (\text{B3})$$

Analogously, in Fig. 13,

$$p(3.1) = \frac{a_1}{a_0 + a_1} \frac{a_2}{a_0 + a_2},$$

$$p(3.2) = \frac{a_0}{a_0 + a_1} + \frac{a_1}{a_0 + a_1} \frac{a_0}{a_2 + a_2},$$

and

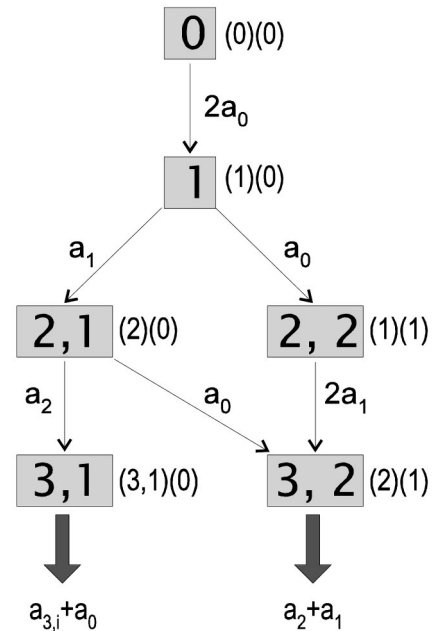


FIG. 13. Top of the primary diagram built from the effective diagram drawn in Fig. 11 (b).

$$\delta_{3,i} = p(3.1) \frac{1}{a_{3,i} + a_0} + p(3.2) \frac{1}{a_1 + a_2}. \quad (\text{B4})$$

As the third term of Eq. (B3) coincides with the second of Eq. (B4), let us reorder Eq. (B3), giving

$$\begin{aligned} \delta_3(\text{exact}) - p(3.3) \frac{1}{a_1 + a_2} \\ = \frac{a_1}{(a_0 + a_1)(a_0 + a_2)} \left(\frac{\gamma_1}{a_0 + \Gamma_1} + \frac{\gamma_2}{a_0 + \Gamma_2} \right) \end{aligned}$$

and similarly in Eq. (B4), obtaining

$$\delta_{3,i} - p(2.2) \frac{1}{a_1 + a_2} = \frac{a_1 a_2}{(a_0 + a_1)(a_0 + a_2)} \left(\frac{1}{a_{3,i} + a_0} \right).$$

To simplify the comparison, let us define two new functions,

$$\begin{aligned} \Delta_3(\text{exact}) &\equiv \left(\delta_3(\text{exact}) - p(3.3) \frac{1}{a_1 + a_2} \right) \frac{(a_0 + 1)(a_0 + a_2)}{a_1} \\ &= \frac{\gamma_1}{a_0 + \Gamma_1} + \frac{\gamma_2}{a_0 + \Gamma_2}, \end{aligned} \quad (\text{B5})$$

$$\begin{aligned} \Delta_3(i) &\equiv \left(\delta_{3,i} - p(2.2) \frac{1}{a_1 + a_2} \right) \frac{(a_0 + 1)(a_0 + a_2)}{a_1} \\ &= \frac{a_2}{a_0 + a_{3,i}}. \end{aligned} \quad (\text{B6})$$

Thus, the Δ 's represent the δ 's after adding an equal term, and multiplied by an equal factor. It is interesting to observe the effect produced by the fusion of block 3,1 and block 3,2 from an algebraic point of view: the sum of the two fractions of Eq. (B5) has converted into the fraction at the right of Eq. (B6). In the case of $\Gamma_1 = \Gamma_2$, $\Delta_3(\text{exact}) = \Delta_3(i)$. In other words, if $\Gamma_1 = \Gamma_2$ that fusion is exact.

To deal with the arithmetic mean, let us define

$$f(x) = \frac{a_2}{a_0 + x} \quad (\text{B7})$$

($a_0, a_2 > 0$), which is concave; this implies that $f(\lambda_1 \Gamma_1 + \lambda_2 \Gamma_2) \leq \lambda_1 f(\Gamma_1) + \lambda_2 f(\Gamma_2)$, where $\lambda_1 \equiv \gamma_1/a_2$, $\lambda_2 \equiv \gamma_2/a_2$, $\lambda_1 + \lambda_2 = 1$, and therefore

$$\frac{a_2}{a_0 + \left[\frac{\gamma_1}{a_2} \frac{1}{\Gamma_1} + \frac{\gamma_2}{a_2} \frac{1}{\Gamma_2} \right]} \leq \frac{\gamma_1}{a_0 + \Gamma_1} + \frac{\gamma_2}{a_0 + \Gamma_2},$$

which means that $\Delta_3(\text{AM}) \leq \Delta_3(\text{exact})$ and therefore $\delta_3(\text{AM}) \leq \delta_3(\text{exact})$.

To deal with the geometric mean, let us in Eq. (B7) make the change of variable $z = \ln x$, then

$$f(x) = \frac{a_2}{a_2 + x} \equiv g(z) = \frac{a_2}{a_0 + e^z},$$

which is also a concave function in z . Hence we have

$$\lambda_1 \frac{a_2}{a_2 + e^{z_1}} + \lambda_2 \frac{a_2}{a_2 + e^{z_2}} \geq \frac{a_2}{a_0 + e^{(p_1 z_1 + p_2 z_2)}};$$

$$\frac{\gamma_1}{a_0 + \Gamma_1} + \frac{\gamma_2}{a_2 + \Gamma_2} \geq \frac{a_2}{a_0 + (e^{\ln z_1})^{\lambda_1} (e^{\ln z_2})^{\lambda_2}} = \frac{a_2}{a_0 + \Gamma_1^{p_1} \Gamma_2^{p_2}}.$$

Thus $\Delta_3(\text{GM}) \leq \Delta_3(\text{exact})$ and $\delta_3(\text{GM}) \leq \delta_3(\text{exact})$.

Finally, for the higher bound we will make in Eq. (B7) the change of variable $z = 1/x$:

$$f(x) = \frac{a_2}{a_2 + x} \equiv h(z) = \frac{a_2 z}{a_0 z + 1}.$$

$h(z)$ is a convex function in z , therefore

$$h(\lambda_1 z_1 + \lambda_2 z_2) \geq \lambda_1 h(z_1) + \lambda_2 h(z_2),$$

and in terms of our ordinary variables this implies

$$\begin{aligned} \Delta_3(\text{HM}) &\equiv f\left(\frac{1}{\frac{p_1}{\Gamma_1} + \frac{p_2}{\Gamma_2}}\right) \geq p_1 f(\Gamma_1) + p_2 f(\Gamma_2) \\ &= \Delta_3(\text{exact}) \end{aligned}$$

and hence $\delta_3(\text{HM}) \geq \delta_3(\text{exact})$.

Note that the argument presented is valid for the δ_3 of any n of coordination $c = 2$ and for both the power-law breaking rule and for the exponential breaking rule.

- [1] *Statistical Models for the Fracture of Disordered Media*, edited by H.J. Herrmann and S. Roux (North Holland, Amsterdam, 1990).
 [2] M. Duxbury, in Ref. [1], pp. 189–228.
 [3] D. Stauffer and A. Aharony, *Introduction to Percolation Theory*, 2nd ed. (Taylor and Francis, London, 1994); M. Sahimi, *Applications of Percolation Theory* (Taylor and Francis, London, 1994).
 [4] L. de Arcangelis, S. Redner, and H.J. Herrmann, *J. Phys. (France) Lett.* **46**, L585 (1985).
 [5] S. Feng and P.N. Sen, *Phys. Rev. Lett.* **52**, 216 (1984); Y.

- Cantor and I. Webman, *ibid.* **52**, 1891 (1984).
 [6] S. Roux and E. Guyon, *J. Phys. (France) Lett.* **46**, L999 (1985).
 [7] H.E. Daniels, *Proc. R. Soc. London, Ser. A* **183**, 404 (1945).
 [8] B.D. Coleman, *J. Appl. Phys.* **28**, 1058 (1957); **28**, 1065 (1957).
 [9] W. Weibull, *Proc. Ing. Vetenskapakad* **151**, 163 (1939).
 [10] B.D. Coleman, *Trans. Soc. Rheol.* **2**, 195 (1958).
 [11] S.L. Phoenix and L. Tierney, *Eng. Fract. Mech.* **18**, 193 (1983).
 [12] E.U. Okoroafor and R. Hill, *J. Mater. Sci.* **30**, 4233 (1995).

- [13] D. Hull, *An Introduction to Composite Materials* (Cambridge University Press, Cambridge, England, 1981).
- [14] D.L. Turcotte, R.F. Smalley, and S.A. Solla, *Nature* (London) **313**, 617 (1985); R.F. Smalley, D.L. Turcotte, and S.A. Solla, *J. Geophys. Res.* **90**, 1894 (1985).
- [15] W.I. Newman, D.L. Turcotte, and A.M. Gabrielov, *Phys. Rev. E* **52**, 4827 (1995).
- [16] R.L. Smith and S.L. Phoenix, *J. Appl. Mech.* **48**, 75 (1981).
- [17] D.G. Harlow and S.L. Phoenix, *J. Compos. Mater.* **12**, 195 (1978); **12**, 314 (1978); R.L. Smith, *Proc. R. Soc. London, Ser. A* **372**, 539 (1980).
- [18] D.G. Harlow, *Proc. R. Soc. London, Ser. A* **397**, 211 (1985).
- [19] L. Tierney, *Adv. Appl. Probab.* **14**, 95 (1982).
- [20] Ch. Kuo and S.L. Phoenix, *J. Appl. Probab.* **24**, 137 (1987).
- [21] S.L. Phoenix and R.L. Smith, *Int. J. Solids Struct.* **19**, 479 (1983).
- [22] W.I. Newman and A.M. Gabrielov, *Int. J. Fract.* **50**, 1 (1991).
- [23] W.I. Newman, A.M. Gabrielov, T.A. Durand, S.L. Phoenix, and D.L. Turcotte, *Physica D* **77**, 200 (1994).
- [24] D. Sornette and C. G. Sammis, *J. Phys. I* **5**, 607 (1995).
- [25] H. Saleur, C. G. Sammis, and D. Sornette, *J. Geophys. Res.* **101**, 17 661 (1996).
- [26] J.B. Gómez, M. Vázquez-Prada, Y. Moreno, and A.F. Pacheco, *Phys. Rev. E* **59**, R1287 (1999).
- [27] J.B. Gómez, Y. Moreno, and A. F. Pacheco, *Phys. Rev. E* **58**, 1528 (1998).
- [28] G. Klambauer, *Aspects of Calculus* (Springer Verlag, New York, 1986).
- [29] W. I. Newman (unpublished).